Tutor/s

Dra. Anna de Juan Capdevila
Departament d'Enginyeria Química i Química Analítica

Dra. Mónica Marro Sánchez
Institute of Photonic Sciences (ICFO)

Grau de Química

Treball Final de Grau

Fluorescence imaging applied to the study of plant tissues.

Imagen hiperespectral de fluorescencia aplicada al estudio de tejidos vegetales.

Adrián Gómez Sánchez

January 2018

Universitat de Barcelona

B:KC Barcelona Knowledge Campus
Campus d'Excel·lència Internacional

Aquesta obra esta subjecta a la llicència de:
Reconeixement–NoComercial-SenseObraDerivada

http://creativecommons.org/licenses/by-nc-nd/3.0/es/

En especial a Silvia, Victor, Rodrigo y Sanae, por toda la ayuda prestada y por haberme hecho sentir tan cómodo con vosotros. A Enric y Maria, por su paciencia y ayuda. A Mónica y a Anna, por la motivación que me han dado y su dedicación. A Jesús Ramoneda, por todos los consejos.

Y, por último, a mi familia y amigos por el apoyo recibido.

Gracias.

REPORT

CONTENTS

1. SUMMARY 3
2. RESUMEN 5
3. INTRODUCTION 7
3.1. Environmental omics. The context of this work 7
3.2. Oryza Sativa 8
3.2.1. Morphology and cross-section 8
3.2.2. Effect of contaminants in Oryza Sativa 10
3.3. Hyperspectral imaging 10
3.4. Fluorescence imaging 11
4. OBJECTIVES 14
5. EXPERIMENTAL 15
5.1. Rice growth 15
5.2. Sample preparation. OCT – based protocol 16
5.3. Image acquisition 17
5.4. Experimental design 18
6. DATA TREATMENT 18
6.1. Data preprocessing 18
6.2. Chemometric tools 21
6.2.1. Image data structure 21
6.2.2. Multivariate Curve Resolution — Alternating Least squares (MCR – ALS) 22
7. RESULTS AND DISCUSSION 25
7.1. Morphological study between control and contaminated plant population 25
7.2. Sample sections and image optimization 25
7.3. Fluorescence image analysis results 27
8. CONCLUSIONS 37
9. REFERENCES AND NOTES 39
APPENDIX 43
Appendix: Distribution maps of control and contaminated plant populations 44

1. SUMMARY

Plant tissues have natural fluorophores on their structure. When plants are exposed to an environmental stress, plant morphology, structural elements and content of fluorophores may vary. Three population of Oryza Sativa (rice) samples grew under control and stress conditions (watered with cadmium 50 µM and 1000 µM solutions). Fluorescence imaging allowed monitoring natural fluorophores such as chlorophylls or lignins in leave tissues. The information from fluorescence imaging was interpreted by the chemometric tool multivariate curve resolution alternating least squares (MCR – ALS) method which provides the pure fluorescence signatures and distribution maps of the fluorophores presents in the plants analyzed. Plants exposed to cadmium were more yellow indicating a lower concentration of chlorophylls. In leaves cross-sections, biological structures seem to be weaker than in non-contaminated plants. The leaf length also decreased in Cd-exposed populations. The fluorescence signatures and distribution maps of three types of chlorophyll and two lignin compounds were resolved. The use of fluorescence imaging techniques combined with chemometric tools are useful to obtain relevant biological, morphological and chemical information about compounds presents in plant tissues.

Keywords: Chemometrics, Hyperspectral Imaging, Environmental omics, Plant tissue analysis, Heavy metal contamination.

2. RESUMEN

Los tejidos vegetales contienen fluoróforos naturales en su estructura. Cuando las plantas son expuestas a estresantes ambientales, la morfología de éstas y el contenido de fluoróforos puede variar. Tres poblaciones de Oryza Sativa crecieron bajo condiciones de control y condiciones de estrés (regadas con soluciones de cadmio 50 μM y 1000 μM). El método de imagen por fluorescencia permitió monitorizar fluoróforos naturales como las clorofilas o ligninas en hojas. La información de la imagen por fluorescencia fue interpretada por el método de resolución multivariante de curvas por alternancia de mínimos cuadrados (MCR – ALS), el cual nos permite obtener los espectros puros de fluorescencia y los mapas de distribución de los fluoróforos presentes en las plantas analizadas. Las plantas expuestas a cadmio fueron más amarillas, indicando una menor concentración de clorofilas. En las secciones transversales de las hojas, las estructuras biológicas parecen ser más débiles que en las plantas no contaminadas. La longitud de la hoja fue menor también en las poblaciones expuestas a cadmio. Los espectros de fluorescencia y los mapas de distribución de tres tipos de clorofila y dos compuestos estructurales lígneos fueron resueltos. El uso de técnicas de imagen por fluorescencia combinadas con herramientas quimiométricas parecen ser adecuadas para obtener información biológica, morfológica y química relevante sobre los compuestos presentes en los tejidos vegetales.

Palabras clave: Quimiometría, Imágenes hiperespectrales, Ómica ambiental, Análisis de tejidos vegetales, Contaminación por metales pesados.

3. INTRODUCTION

3.1. ENVIRONMENTAL OMICS. THE CONTEXT OF THIS WORK

Environmental omics is a science field oriented to acquire knowledge of how environmental factors affects to a biological organism and how biological organism develop a response to both acute and chronic stress factors exposure. The suffix -ome is used to address the objects or compounds of study as an organism and not as individual pieces (from the Greek -oma ωμα, which indicates *whole*). Within the –omics context, we can find know denominations as genome, proteome or metabolome according to the family of biological compounds studied.

This work follows the general lines of the European project Chemometric and High-throughput Omics Analytical Methods for Assessment of Global Change Effects on Environmental and Biological Systems (CHEMAGEB), whose purpose is generally the use of chemometric methods to evaluate the effects of changes in the environment and climate in target biological systems that are representative of ecosystems. More specifically, the aim of this work is to analyze changes generated in a biological sample by the exposure to heavy metals using hyperspectral imaging combined with chemometric tools.

Applying a destructive-analytical technique in a biological system modifies both structure and spatial distribution of the metabolites and this generates a requirement: non-destructive techniques for the acquisition of complete data. High-efficiency chromatography can give us precise results about the amounts and types of components present in a biological sample, but it destroys the spatial information, i.e., it does not provide information about the distribution of the components in their natural environment. Thus, hyperspectral imaging allows analysing the biological system observing the natural behaviour of the components in their own environment and how they react under a stress situation. Hyperspectral imaging is a non-destructive technique and preserves the sample morphology[1].

In our case, we focused on the use of Oryza Sativa Japonica Nipponbare, a rice variety, as a biological sample and the study of change in their fluorophores by the exposure to heavy metals.

3.2. ORYZA SATIVA

3.2.1. Morphology and cross-section

Oryza sativa, commonly called rice, is a semi-aquatic species belonging to the family of grasses. Its seed is edible and forms the basis of the diet of a large part of the world population. It is the second most produced cereal in the world, after corn. Rice contributes very efficiently to the caloric intake of the diet being responsible for the caloric intake of a fifth of calories consumed in world by humans. In countries as Bangladesh and Cambodia it can be almost three quarters of the population diet. These characteristics are in spotlight in terms of its production performance and nutritional and caloric contribution[2].

Rice is an annual plant, with cylindrical and fistulous stems with nodes and internodes 40-150 cm high at maturity. Lower part of the stem usually floats in the water, while the upper part is erect. The mature roots are fibrous, with secondary roots and hairs. Leaves are sessile, slightly rough to touch, they have flat blade and are attached to the stem by the pod. Leaves are distributed alternately along the stem. They are lanceolate, finished in tip, with parallel nerves and make 5-10 mm wide. The flowers are small and their fruit are a kind of achene of white compressed ovoid. The seed is covered with a multilayer husk. What is known as rice grain is the endosperm (therefore, devoid of the embryo) of this seed[3] (Fig. 1).

Cross section of leaf presents an interesting morphology: vascular system of the plant becomes patent, being able to observe the different conduits that the plant develops for the transport of water, minerals and nutrients. A cross section 20 µm thickness allows observing the xylem and the phloem. The function of first one is transport minerals and water, the second one transports the sugars inside the vegetal tissues. Cuticle and epidermis protect the internal parts of the plant of external damages. Finally, there are spongy tissue which is formed by parenchyma cells, collenchyma cells, sclerenchyma cells and bundle sheath cells[4,5] (Fig. 2).

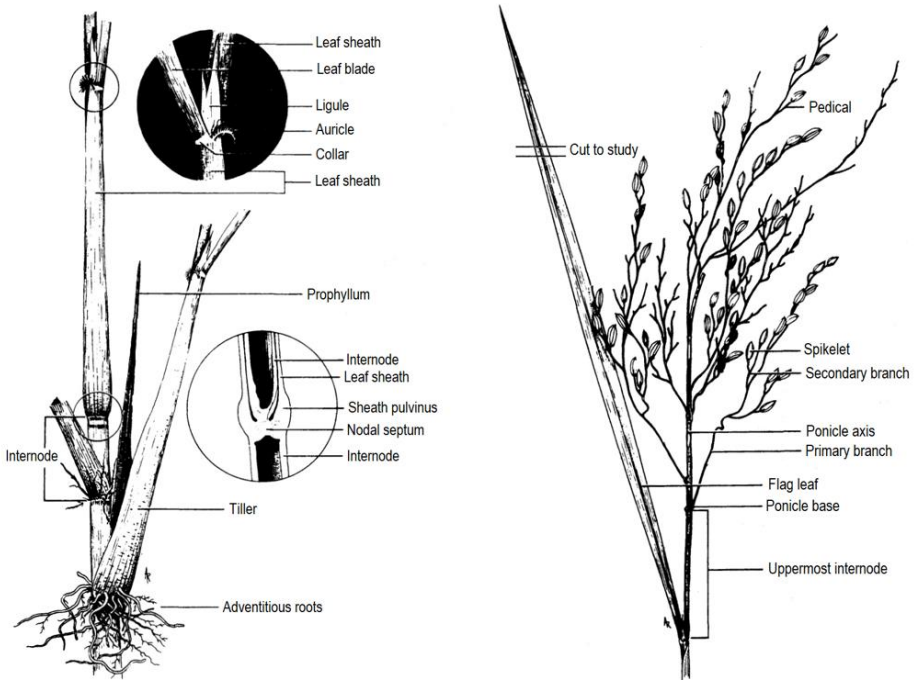

Fig. 1 Oryza Sativa morphology. Reproduced from Chang, T.-T.; Bardenas, E. A. The Morphology and Varietal Characteristics of the Rice Plant. Tech. Bull. 4 1965, 40.

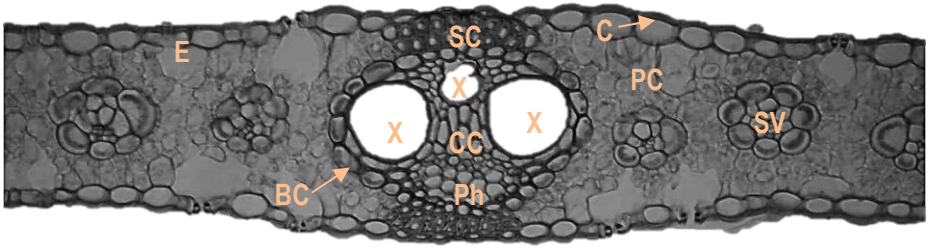

Fig. 2 Oryza Sativa morphology of cross section. Epidermis (E), Cuticle (C), Phloem (Ph), Xylem (X), Parenchyma cells (PC), Collenchyma cells (CC), Sclerenchyma cells (SC), Bundle sheath cells (BC), Secondary Vein (SV). Images extracted from *The Daily Plant*.

The epidermis and vessel cells have lignified cell walls, which gives them resistance and allow them to be efficient in their function. In addition, the epidermis contains hydroxycinnamic acids, as coumaric acid, ferulic acid or sinapinic acid, that absorbs ultraviolet radiation, protecting the

plant from harmful electromagnetic radiation[6,7]. On the other hand, parenchyma cells are thin-walled cells that occupy the vast majority of the interior space. They contain the chloroplasts, organelles that allow photosynthesis through membrane protein systems in thylakoids. In the thylakoids there are several molecules that emit fluorescence, such as chlorophyll A, chlorophyll B and accessory pigments as carotenoids. Carotenoids absorb light in the blue region of the spectrum, and the energy absorbed can be transferred to chlorophylls, achieving more energy to use in photosyntesis[8].

3.2.2. Effect of contaminants in Oryza Sativa

In the context of environmental metabolomics, the interaction between biological organism and the environmental contaminant is studied. In this particular case, cadmium has the role of an environmental stressor. Cadmium is a heavy metal that can be considered toxic, and its impact on the number of active fluorophores can be detected. It has been reported that concentrations of the order of 10^{-6} M in water that are absorbed by the roots of the plant decrease the amount of several fluorophores such as chlorophyll A and chlorophyll B active, turning the plant yellow. But neither in the light harvesting complex (a protein system with the aim of realize the photosynthesis) nor in the carotenoids have been significant effects[9].

On the other hand, the exposition to heavy metals in plants has effects in morphology. Dark deposits in the endodermal cells and vascular cylinder were observed that obstruct the plant vascular cylinders. The rupturing of tissue is habitual and plant growing is slowed down[10].

3.3. HYPERSPECTRAL IMAGING

Electromagnetic spectrum offers different information depending of the wavelength range used and the optical phenomenon studied. The absorption, emission or excitation spectra are formed from the accumulation of discrete responses at different excitation wavelengths. When we obtain spectra of techniques such as infrared, Raman or fluorescence, the instrumental response is generally composed of a single global spectrum because the measurement is obtained at a single point. This is useful if the sample meets with several characteristics, such as being homogeneous and having the ability to correctly extrapolate the spectrum to any spatial point in the sample. However, biological tissues do not have these proprieties. Spatial information on biological samples allows drawing a more detailed map of the true nature of the analytes of interest. For example, to study the accumulation of a toxic substance in a living organism, spatial

information is required to know where is accumulated or if there is any difference caused by the contaminant at a tissue level. In addition, we can complete the spatial information (dumped in a plane, of coordinates x and y) with a third coordinate: the spectral coordinate. Each point in the plane (image) has associated a full spectrum, which generates a cube of information; x and y as spatial coordinates and λ as the spectral coordinate. This analytical spectroscopic technique is called hyperspectral imaging (Fig. 3). Thus, a hyperspectral image is an analytical measurement that offers spatial and spectral information on samples.

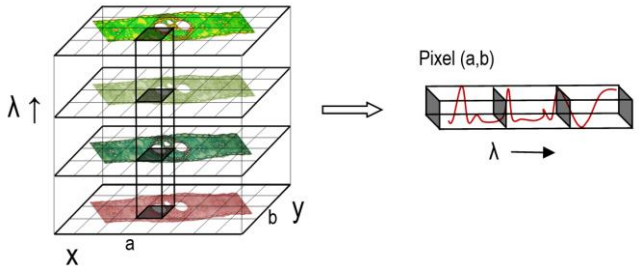

Fig. 3 Illustration of a hyperspectral image. On the left, a cube formed by the spatial coordinates x and y that make up the image, and λ as the spectral coordinate. On right, a pixel with its corresponding spectrum formed with several responses at different wavelengths.

3.4. FLUORESCENCE IMAGING

Fluorescence spectroscopy uses the phenomenon of fluorescence to acquire information about the nature of the compounds present in a sample.

When a molecule is illuminated with a light source of a certain wavelength, photons are absorbed and electrons are excited into more energetic electronic states. In that situation, electrons can decay to less energetic vibrational states without emission by a phenomenon known as "relaxation." When this happens, electrons, upon returning to its fundamental electronic state, emit a photon with a longer wavelength than absorbed (Fig. 4).

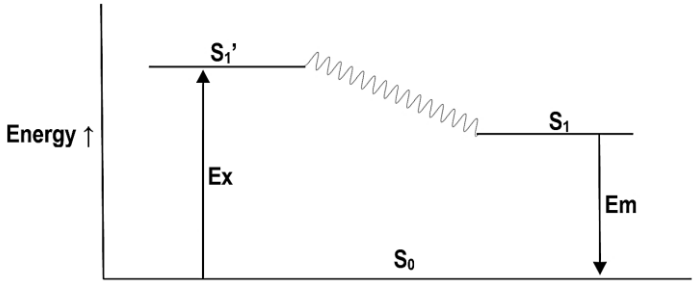

Fig. 4 Jablonski diagram of fluorescence phenomena.

This emission, less energetic than the light used to excite, is captured by detectors that filter by wavelengths the emitted radiation. Thus, an emission spectrum is constructed by acquiring the radiation emission and classifying it according to its wavelength along the electromagnetic spectrum.

There are molecules capable of reproducing this phenomenon in living beings called fluorophores. Generally, if one molecule has electrons that can delocalize, it is probably fluorescent. Many plant pigments such as carotenes, different chlorophylls and some proteins show fluorescence.

Hyperspectral fluorescence images are produced by scanning the sample surface and obtaining a fluorescence spectrum per pixel. That is, each pixel that forms the image has an associated fluorescence emission spectrum. All pixel spectra form the data cube of the hyperspectral image. The image is obtained by acquiring individual frames on the full sample surface at each emission wavelength. All frames together form the image.

Maximum emission peaks of several fluorophores found in plant leaves are described in Table 1.

Fluorescent compound[11]	Emission peak (nm)	Location
Chlorophyll A	685[12]	Parenchyma cells
Chlorophyll B	652[13], 680[14]	Parenchyma cells
Ferulic acid	415[15]	Cell walls, Collenchyma cells Sclerenchyma cells, epidermis
p-Coumaric acid	400[7]	Cell walls, Collenchyma cells Sclerenchyma cells, epidermis
Chlorogenic acid	440-455[16]	Cell walls, Collenchyma cells Sclerenchyma cells, epidermis
Caffeic acid	440-455[16]	Cell walls, Collenchyma cells Sclerenchyma cells, epidermis
Beta-carotene	550[17]	Parenchyma cells
Lignin	500-600[18]	Cell walls, Collenchyma cells Sclerenchyma cells, epidermis

Table 1. Fluorophores present in plant leaves, their emissions peak and their locations in leaves.

One of the techniques used to acquire fluorescence images is the use of a confocal microscopy. A classical fluorescence microscope would generate an intermediate image by an objective lens, containing both focal and out-of-focus signal emanated by the sample. When out-of-focus planes are collected by the detector, the resolution decreases. Instead, the confocal microscope uses an optical imaging technique to increase spatial resolution and reconstructs three-dimensional images using a spatial "pinhole" (delimiting orifice collimator) to eliminate the unfocal light or flashes of lens coming from samples thicker than the focal plane (Fig. 5).

When imaging a single spot, the detector will record both a spot-shaped feature from the focal plane and extended blurry discs from other regions. By introducing a pinhole aperture in the intermediate image plane, nearly all out-of-focus signal is cut off and solely the emission from the focal plane can reach the detector. This technique allows us gaining spatial resolution due to a better focus on the focal plane.

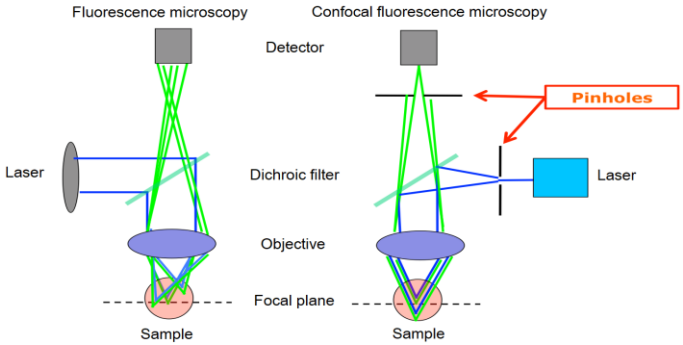

Fig. 5 Simplified schema of fluorescence confocal microscopy and classical fluorescence microscopy. Illustration from *Principia.io*, by Daniel Moreno.

4. OBJECTIVES

Oryza Sativa is a typical and important plant for the society. The fluorophores can be a health indicator of the plant and can be useful to check the sensitivity to contamination of some heavy metals. The objective of this work is developing a protocol to obtain spatial, quantitative and qualitative information about significant fluorophores through confocal fluorescence microscopy and chemometric analysis. This combination of techniques and data treatment improves the quality of the information obtained. As an additional benefit, these new techniques are minimally invasive, fast and do not generate chemical residues.

It is the first time that this combination of techniques is used to analyze rice plant tissues. For this purpose, it is necessary the optimization of sample treatment stages and instrumental parameters to obtain satisfactory hyperspectral fluorescence images and suitable interpretations through chemometric data analysis. Therefore, this work has three objectives:

a) To optimize instrumental parameters of fluorescence confocal microscopy to achieve satisfactory hyperspectral images of plant tissues.

b) To design a data treatment that includes appropriate data processing and correct use of the Multivariate Curve Resolution - Alterning Least Squares (MCR-ALS) method to obtain the pure spectral signatures of the components of the sample and their distribution maps, and

c) To perform a qualitative study of the effects of cadmium-contaminated water on the concentration and distribution of fluorophores in Oryza Sativa using hyperspectral images of a population of control rice, a population of rice exposed to 50 µM cadmium solution and a population of rice exposed to 1000 µM solution.

5. EXPERIMENTAL

5.1. RICE GROWTH

Plant growth was performed using a procedure previously described[19]. Oryza Sativa Japonica Nipponbare seeds, a common variety of rice, were obtained from the Center for Research in Agricultural Genomics (CRAG) at Autonomous University of Barcelona and were germinated for 2 days at 30 ºC in a wet environment. This method allows obtaining quickly germinated seeds ready to grow. After germination, seeds were grown for 22 days under controlled conditions in an Environmental Test Chamber MLR-352H (Panasonic®). Conditions are described in Figure 6 and mimic natural daylight cycles.

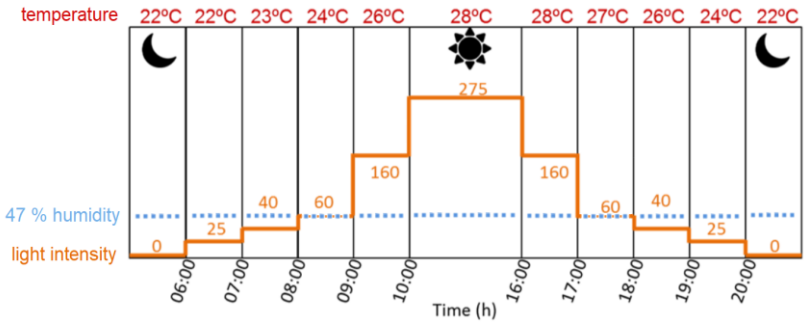

Fig. 6 Conditions used in rice growth.

Three different rice populations were grown: a control population watered 3 times a week with 150 ml of mili-Q water for 22 days. Another population watered 3 times a week with 150 ml of mili-Q water for the first 10 days and after watered with a 150 ml of 50 µM solution of Cd^{2+} until day 22. The last population was watered 3 times a week with 150 ml of mili-Q water for the first 10 days and the remaining time with 150 ml of 1000 µM solution of Cd^{2+}.

After harvest, some parts of rice plants such as leaves and stems were collected for further study.

5.2. SAMPLE PREPARATION.

In this study, OCT – protocol was tested to optimize the preparation and cryosectioning of Oryza Sativa and to achieve adequate hyperspectral images of vegetal tissue of the leaves. This protocol is based on the use of *Tissue – Tek optimum cutting temperature compound* (OCT) as embedding medium, described previously for cryosections of animal tissues[20].

OCT is a polymer based on water soluble glycols and resins typically used in microscopy for sample preparations. At room temperature is viscous, but at -15 ºC is solid. These properties are good to fix the sample. Also, OCT does not penetrate on the sample and respects the natural state of vegetal tissues.

To carry out this protocol, we picked a plant of a certain population randomly and we cut a piece of a leaf (at middle of leaf) of 1 cm long, and we transferred to a cryomold support with OCT. Finally, when the sample was inside of the polymer totally embedded, we did a flash freezing with liquid nitrogen. This method allows us freezing quickly the sample avoiding the creation of big crystals which can damage the sample and allows a long sample preservation. The frozen samples were stored at -80 ºC until they were cut. To obtain cuts of 20 µm thickness, we used a

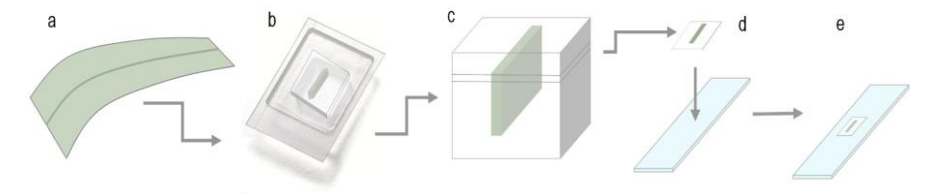

Fig. 7 Scheme of OCT protocol. a) Cut of leaf of 1 cm long. b) Embed sample in OCT. c) OCT cube frozen. d) Leaf cryosection and fix in a slide. e) Measurement.

microtome cryostate at the Parc Científic of Barcelona in a temperature range of -20 ± 5 ºC. The cryosections obtained were transferred on a slide support and covered with a coverslip and stored at 4 ºC until the measurement (Fig. 7).

5.3. IMAGE ACQUISITION

The measurements were carried out using a fluorescence confocal microscope (CW STED, Leica) at the Institut de Ciències Fotòniques (ICFO) with a 10x objective. There are several parameters that we can modify to achieve a good instrumental response: pinhole size, exposure time, frame accumulation, laser power and excitation wavelength. Below, an explanation of the effect of modifying these parameters and a description of the final optimal set up is provided.

- The pinhole, in confocal microscopy, is a little orifice by which unfocal light is filtered. A small pinhole increases the spatial resolution but decreases the intensity of the instrumental response. Instrumental response was sufficient to close the pinhole to minimal size, gaining resolution (pinhole size 53 µm). The pixel size was 704 × 704 nm^2 to control population and 957 × 957 nm^2 to exposed population. The difference of spatial resolution is explained by the use of two different zooms during the acquisition in order to obtain better images.
- Exposure time is the time during which the detector collects the instrumental response. An increase of exposure time leads to an increase of the intensity response. Exposure time per individual frame was fixed at 100 Hz.
- Frame accumulation allows adding the response of several scans and reduces the random instrumental noise. In contraposition, the measurement time is increased. Frame accumulation was fixed at 1. The fluorescence intensity was sufficient with 1 frame accumulated.
- Laser power determines the number of excitation photons. If a higher number of photons impacts a sample, a higher number of electrons will be excited. In consequence, a higher number of photons are reemitted as fluorescence and the signal intensity increases. The fluorescence confocal microscope has several discrete lasers with different power. Power laser was fixed at 100 %. The intensity response was adequate using an argon laser with 488 nm excitation wavelength at 100 % of power (1.09×10^{-3} W).

- Excitation wavelength was fixed at 488 nm. The laser with 488 nm excitation wavelength was selected to achieve the widest wavelength range of detection (498 to 760 nm) and the higher power. Several fluorophores such as chlorophylls and lignins emit around 500 – 800 nm.

5.4. EXPERIMENTAL DESIGN

In order to achieve representative results, an experimental design to acquire the fluorescence images was proposed. The finality of experimental designs is to interpret correctly the results of the cadmium exposure and no attributing it to other factors. 24 cryosections were acquired in a random sequence from the three populations grow: 8 from control, 8 from exposed population with 50 µM and 8 from exposed population with 1000 µM (Fig. 8). For ever populations, two different plants were selected; two different leaves from each plant and two cuts from every leaf. All the selections were done randomly. Only 18 out of a total of 24 cryosections were measured. However, 18 cryosections are enough to achieve a representative results.

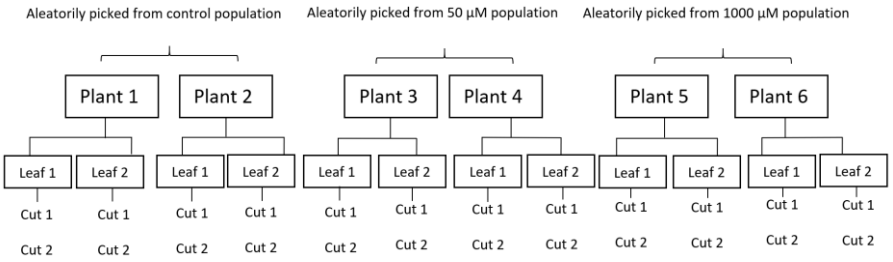

Fig. 8 Experimental design followed to achieve a representative set of samples. Only 18 out of a total of 24 cryosections acquired were measured.

6. DATA TREATMENT

6.1. DATA PREPROCESSING

Data preprocessing involves all data analysis techniques whose purpose is to improve the quality of a data set before applying any chemometric tools. As a result, we can reduce sources

of variation that are not related to chemical or biological information. If data preprocessing is not done, it can be difficult to interpret correctly the information obtained. Fluorescence spectra have no problems of baseline as Raman o NIR spectra can have. The hyperspectral image obtained from a fluorescence measurement has approximately 512 × 512 × 88 fluorescence intensity measurements: 512 × 512 are the pixel number x and y directions and 88 is the pixel number for the spectral channel.

The number of spectra collected is more than 260,000 per one image. This data size contains a lot of unnecessary information, as the background pixels. Select and separate the biological and chemical information from useless information is important to achieve less computation time when chemometrics techniques are used. In addition, the quality of the results obtained improves with MCR – ALS algorithm (which is explained afterwards), if only sample information is used.

To reduce the computation time, we used three algorithms with MATLAB R2016a software. The first one, called "binning", allows to combine pixels to reduce the final size of the hyperspectral image. For example, if we want to reduce the matrix size from 10 × 10 to 5 × 5, a pixel of the binned image will be the result of summing 2 × 2 pixels of the original image (Fig. 9). This function is useful to gain computation time, but it lowers the spatial resolution of images. For all hyperspectral images obtained from samples, the binning was 2 × 2 for spatial dimension.

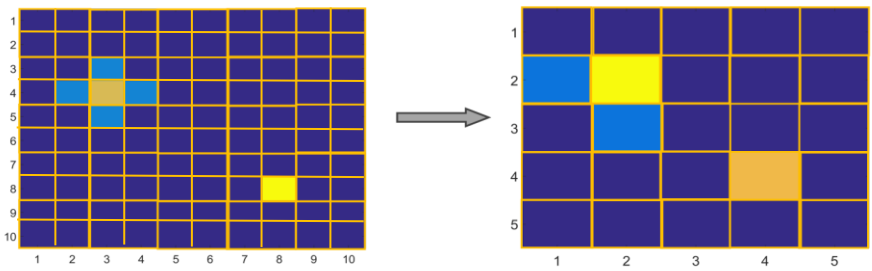

Fig. 9 An example of binning image function. On the left, data matrix A with 10x10 size. On the right, B data matrix binned by a factor of 2.

The second algorithm is used to separate the image background pixels from the pixels of biological sample. This function allows us obtaining a data matrix much smaller than the original data matrix, accelerating the posterior calculus with chemometric tools. The background image sets a threshold according to the intensity response of each spatial pixel. All pixels having total emission intensity lower than the threshold are not used for further analysis (Fig. 10).

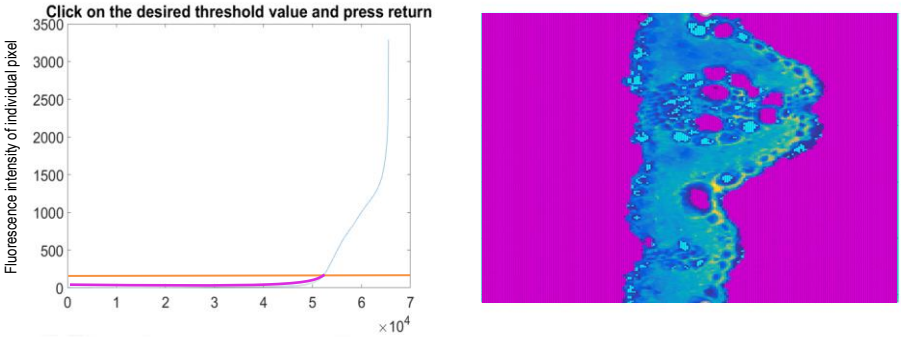

Fig. 10 On the left, interface algorithm to cut the background pixels. The vertical axis represents the total emission intensity, and the horizontal axis each pixel. Threshold is set as a function of the pixel intensity (orange). The pixels under the threshold are discarded. On the right, preprocessed image: binned and without background pixels (purple).

Finally, a third algorithm is used to smooth the spectra using the Savitzky–Golay filter algorithm[21] (Fig. 11). This algorithm works replacing each point in the spectra with the grade n polynomial interpolation of m neighbouring points, where m is a positive integer called the "smooth width". Usually m is an odd number. In this case, $n = 2$ and $m = 7$ was selected to use this algorithm. This preprocessing method is applied to all images collected.

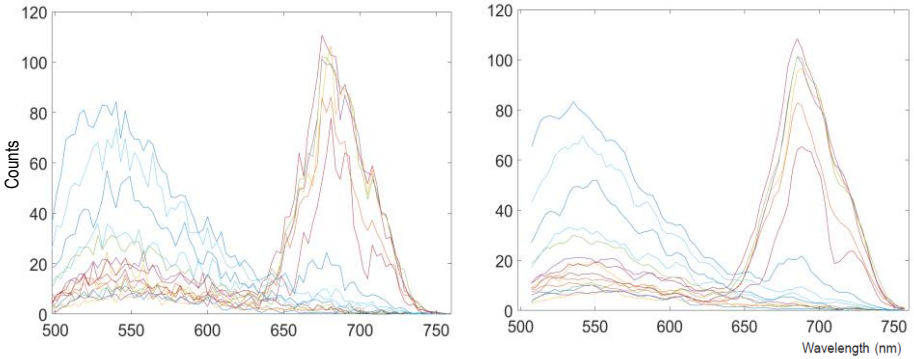

Fig. 11 On the left, raw spectra collected. On the right, smoothed spectra using the Savitzky–Golay filter algorithm.

6.2. CHEMOMETRIC TOOLS

6.2.1. Image data structure

The image obtained can be represented as a data cube with x and y as spatial pixel coordinates and λ as spectral dimension. This cube can be unfolded in to a new data matrix ($\boldsymbol{D}$) which each element is the response at a pixel and wavelength determined. (Fig. 12).

The $\boldsymbol{D}$ matrix englobes all fluorescence emission spectra of the plant tissue. The fluorescence spectra follow a linear law that relates concentration of the fluorophore with the instrumental response with next relation: $I_f = kc$ where c is the sample concentration and k is a constant.

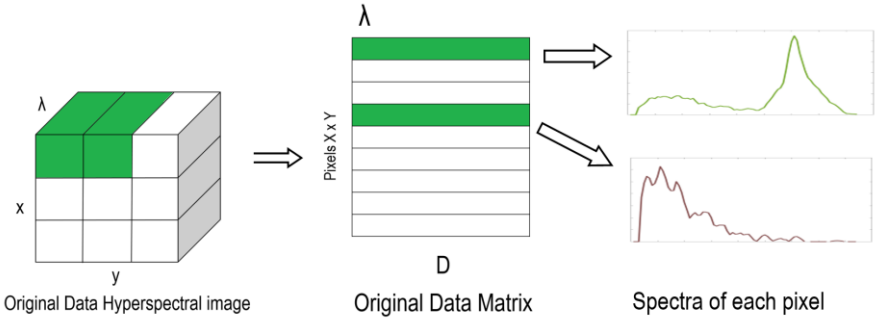

Fig. 11 Hyperspectral image structure and unfolded data cube.

The spectra obtained through different instrumental techniques can be reproduced using the linear equation $I_f = kc$ where each fluorophore of the matrix $\boldsymbol{D}$ is defined as $D_i = k_i(\lambda)\ c_i$ and $k_i(\lambda_i \dots \lambda_n)$ define a unit pure fluorescence spectrum s_i^T. Then, all spectra in matrix $\boldsymbol{D}$ can be defined as sum of all pure spectra contribution weighted by the concentration of compounds in each pixel: $\boldsymbol{D} = \sum c_i\ s_i^T$ where $c_i s_i^T$ term indicates the signal contribution for each fluorophore in the chemical system (Fig. 13). This bilinear model can be rewritten as $\boldsymbol{D} = \boldsymbol{C}\,\boldsymbol{S^T} + \boldsymbol{E}$ where $\boldsymbol{E}$ is an error matrix.

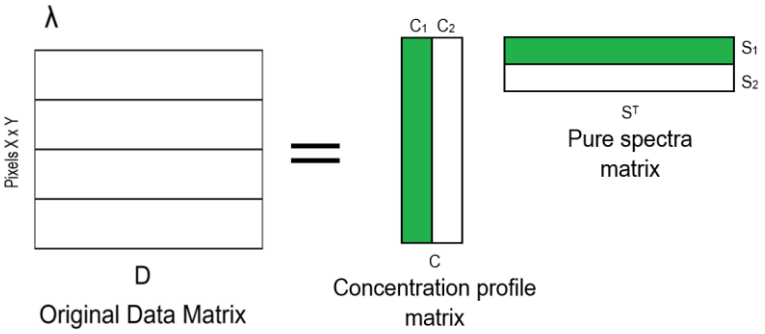

Fig. 12 A bilinear model. D matrix can be explicated with a two-new matrix: concentration profile matrix and pure spectra matrix, following a linear law.

6.2.2. Multivariate Curve Resolution — Alterning Least Squares (MCR – ALS)

In a fluorescence image of a biological sample, only $\boldsymbol{D}$ is known. $\boldsymbol{C}$ and $\boldsymbol{S^T}$ matrices are unknow because the instrumental response is an unknown mixture of each fluorophore contribution. To resolve the problem of mixed components and to decompose the $\boldsymbol{D}$ matrix in to the bilinear model including $\boldsymbol{C}$ and $\boldsymbol{S^T}$, Multivariate Curve Resolution — Alternating Least Squares (MCR – ALS) chemometric method was used in MATLAB R2016a[22]. This method is based in a bilinear decomposition model, and, for this reason, can be used to try to solve the unmixed problem. The objective of this method is decomposing the original data $\boldsymbol{D}$ matrix into the pure spectra $\boldsymbol{S^T}$ and pure concentration profiles $\boldsymbol{C}$ of the sample compounds. To do this, MCR – ALS works using an iterative alternating least squares method as described below.

First, we select a number n of components that form the sample. This number can be based in previous knowledge o can be determined with chemometric tools, such as principal component analysis (PCA)[23]. The next step is selecting an initial estimate for the concentration profiles C or pure spectra S^T of chemical system. To do this, the *simple-to-use interactive self-modelling analysis (*SIMPLISMA)[24] method was used. This algorithm selects the n spectra of the fluorescence image that show the largest difference among them. The n spectra selected corresponds to the most different fluorescence spectra in the original data set ($\boldsymbol{D}$).

Then, according to the $\boldsymbol{D} = \boldsymbol{C}\,\boldsymbol{S^T}$, we can calculate $\boldsymbol{C}$ with least squares method because we have $\boldsymbol{D}$ matrix and the initial estimate for $\boldsymbol{S^T}$.

$$\boldsymbol{C^*} = \boldsymbol{S^{T+}}\,\boldsymbol{D}$$

$$\boldsymbol{S^{T+} = S\,(S^T\,S)^{-1}}$$

After this, $\boldsymbol{S^{T*}}$ is recalculated using the new $\boldsymbol{C}$ matrix with least squares method.

$$\boldsymbol{S^{T*} = D\,C^{+*}}$$

$$\boldsymbol{C^{+} = C\,(C^T\,C)^{-1}}$$

$$\boldsymbol{D^{*} = C^{*}\;S^{T*}}$$

At this point, $\boldsymbol{D^*}$ matrix is compared with the original $\boldsymbol{D}$ matrix. The iterative optimization is finished when the difference among $\boldsymbol{D^*}$ and $\boldsymbol{D}$ is small enough. The convergence criterion was 0.1 % for the difference between the lack of fit (defined below) between for two consecutive iterations. When convergence is achieved, MCR – ALS gives the matrices $\boldsymbol{C}$ and $\boldsymbol{S^T}$ and several parameters that indicate the quality of the model. The results are satisfactory when the difference between original $\boldsymbol{D}$ matrix and the new $\boldsymbol{D^*}$ matrix calculated, using the concentration profile and pure spectra matrix is sufficiently small, according to the convergence criterion established.

Least squares method provides the best solutions in terms of variance explained, which is suitable to describe the natural measurement as well as possible. To ensure that MCR – ALS gives chemically meaningful concentration profiles and the pure spectra of each component, several constraints are established that reflect natural properties of the $\boldsymbol{C}$ and $\boldsymbol{S^T}$ profiles to be resolved. MCR – ALS constraints are also helpful to reduce the ambiguity in the solutions obtained[25].

To assess the model fit, two parameters were considered.

- Percentage of Lack of fit (% LOF)
- Percentage of variance explained by the model (% $\boldsymbol{r^2}$)

$$Lof\,(\%) = 100 \times \sqrt{\frac{\sum_{i,j} e_{ij}^2}{\sum_{i,j} d_{ij}^2}}$$

$$r^2(\%) = 100 \times \left(1 - \frac{\sum_{i,j} e_{ij}^2}{\sum_{i,j} d_{ij}^2}\right)$$

Where d_{ij} is the element of the original $\boldsymbol{D}$ matrix of row i and column j and e_{ij} is the related residual value obtained from the difference between $\boldsymbol{D}$ experimental matrix and $\boldsymbol{D^*}$ model matrix obtained from MCR – ALS.

The criteria to apply a certain constraint depends on the nature of the data and the profiles to be recovered. In our case, fluorescence spectra and concentration profiles never take negative values, and for this reason non-negativity was chosen as a constraint to force the profiles to be formed by positive values. This constraint was applied both to the $\boldsymbol{C}$ and $\boldsymbol{S^T}$ matrix. Finally, the distribution maps of each component in the image can be obtained by refolding each concentration profile according to the original image structure (Fig. 14).

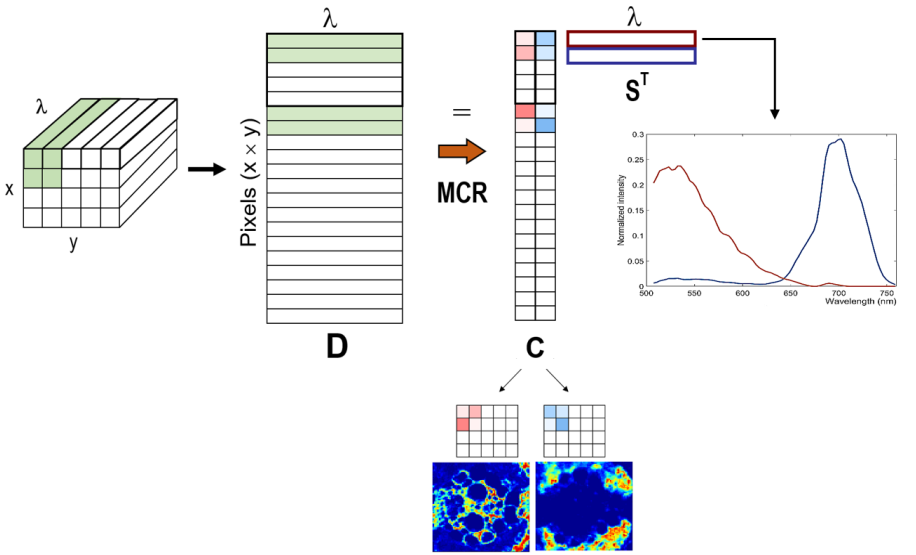

Fig. 14 Representation of a hyperspectral image structure and the obtaining of the pure spectra and distribution maps for two components.

In biological studies, an individual image does not give enough information about all compounds. For this reason, it is needed to enlarge the available information in the system that will be analyzed. If MCR – ALS is applied to a $\boldsymbol{D}$ matrix with much more information (for example, with several hyperspectral images together), an improvement of resolved $\boldsymbol{C}$ and $\boldsymbol{S^T}$ matrices can be achieved. In our case, three separate multisets containing all images of each plant population were built to obtain better resolved pure signatures and maps related that may describe better the general trends of the different plant populations (Fig. 15). The multisets can be built because all hyperspectral images were obtained with the same spectral conditions (wavelength range and spectral resolution). This means that the spectral dimension of $\boldsymbol{D}$ is the same in all images. Contrarily, the pixel direction is free for every image and this means that images with different number of pixels and geometries can be analyzed together. MCR-ALS multiset analysis provides

a single $\boldsymbol{S^T}$ matrix, valid for all images, with the pure spectra of the fluorophores in the plant tissues analyzed and an extended $\boldsymbol{C}$ matrix, with concentration profiles that may be refolded into the maps of each compound in each of the images.

The same constraints used for a single image, i.e., non-negativity for $\boldsymbol{C}$ and $\boldsymbol{S^T}$ were applied in multiset analysis.

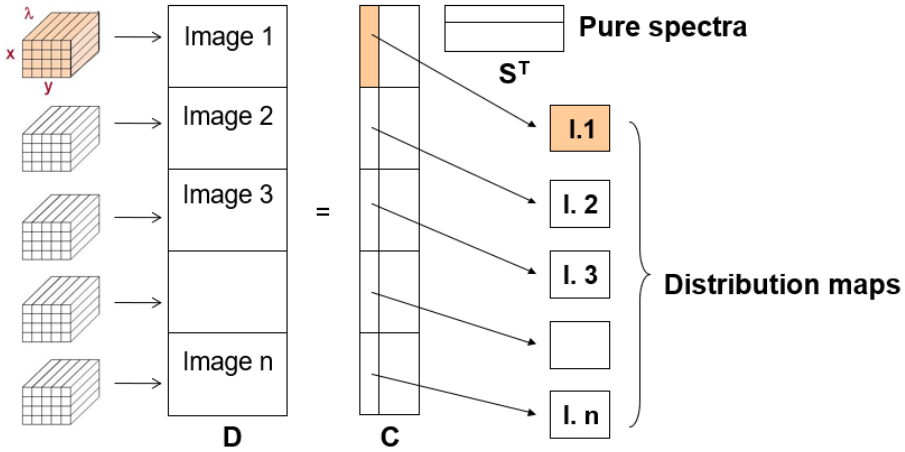

Fig. 15 Multiset structure formed by n hyperspectral images of the same plant population.

7. RESULTS AND DISCUSSION

7.1. COMPARATIVE MORPHOLOGICAL STUDY BETWEEN CONTROL AND CONTAMINATED PLANT POPULATIONS

Rice growth was carried out according to the procedure mentioned in section 5.1. In order to obtain relevant information of the effects of cadmium in the plant growth, a small study about the differences of height and colouration was done. The leaves height of 6 plants of each population were measured. A two-tailed t-students test was realized to observe any significative difference between populations.

It has been found a significant difference in leaves length between control and exposed populations ($p<0.05$). No difference has been found between the plants populations exposed to 50 µM and 1000 µM. ($p>0.95$). These results coincide qualitatively with literature[26].

A difference was found between leaves coloration of control population and leaves coloration of exposed population at a glance. The exposed plants were more yellow than control plants due to a less chlorophyll quantity in leaves. (Fig. 16).

Fig. 16 On the left, leaves of control population. In the centre, leaves of 50 µM solution exposed population. On the right, leaves of 1000 µM solution exposed population.

It seems that, according to *Pagliano C. et al [2009]*[9], cadmium does not affect the photosystems involved in photosynthesis and their structure, but it does over the pigment content and compounds such as chlorophylls and carotenoids.

7.2. SAMPLE SECTIONS

Cryosectioning Oryza Sativa leaves with OCT as embedding medium was carried out according to section 5.2. In contrast to other biological samples, the morphology of the sections was adequate to acquire hyperspectral images (Fig. 17).

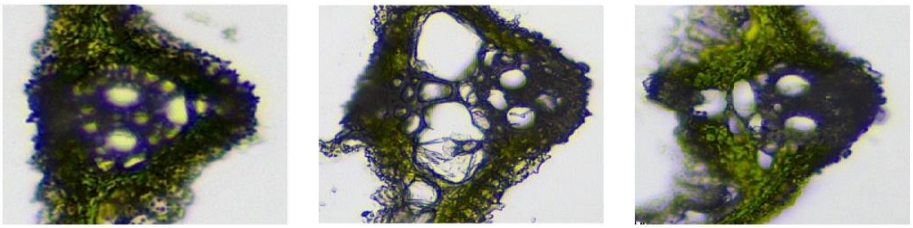

Fig. 17 Principal vessel leaf cryosections obtained by OCT protocol. On the left, a cryosection from control population. In the middle, a cryosection from 50 µM exposed population. On the right, a cryosection from 1000 µM exposed population.

During the cryosectioning, it was noted that the cryosections seemed to be weaker in exposed populations. The morphology was destroyed easily during the sectioning in some cryosections (Fig. 18).

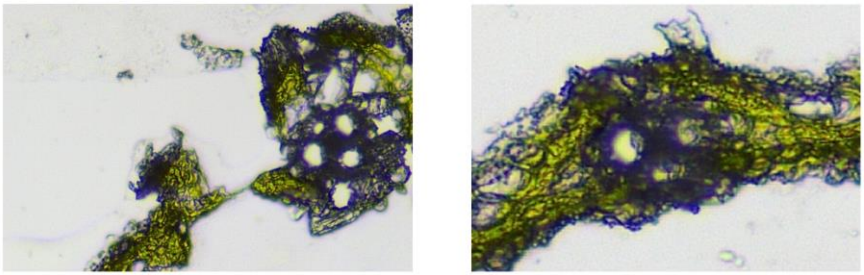

Fig. 18 On the left, an example of broken cryosection of a contamination plant. On the right, a secondary vessel in broken samples.

Usually, fluorescence images are measured in a glass slide, covered with coverslide and sealed with a phosphate-buffered saline (PBS) solution. However, these samples were not measured only by fluorescence imaging. Within our research team, other people were measuring the same samples with Raman imaging after the fluorescence measurement in order to obtain complementary information about the biological compounds of the sample. Since OCT residues could be dissolved in PBS solution and distort Raman signal, the samples have been placed in dried slides with a coverslide without PBS solution to acquire the fluorescence images.

7.3. FLUORESCENCE IMAGE ANALYSIS RESULTS

Only 18 out of a total of 24 cryosections were measured with a fluorescence confocal microscope protocol as described in section 5. The data were preprocessed according the algorithms mentioned in section 6.1.

A previous test using MCR – ALS method on individual images indicated that there are 5 (A, B, C, D and E) components per individual image in the control population. In Cd(II) 50 µM exposed population, 7 components (A, B', C, D', E, F and G) were detected. Finally, 5 components (A, B, C, D and E) were detected in Cd(II) 1000 µM exposed population. Some components detected are common to all populations. To obtain better resolved signatures and concentration profiles, three multisets were formed for each population with 6 images per population.

In Cd(II) 50 µM exposed population, not all components were present in all images. In the MCR – ALS method, we can select and encode which components are present in the different images through a matrix formed by zeros and ones. The next matrix indicates which components are in each image.

	A	B'	C	D'	E	F	G
Image 1	1	1	1	1	1	1	1
Image 2	1	1	1	1	1	1	1
Image 3	1	1	0	0	0	1	1
Image 4	1	1	0	0	0	1	1
Image 5	1	1	1	1	1	1	1
Image 6	1	1	1	1	1	1	1

This matrix is formed by six rows referring to the images that form the multiset, and by seven columns, one per component. Zeros and ones indicates the absence or presence of the component in the image (this is called the correspondence among species constraint)[20,25]. Thus, MATLAB can read which components are present o absent in one image improving the solutions given by MCR – ALS method for this special case, in which not all components are in all images.

Table 2 shows the fit parameters for the three multisets analyzed. All models obtained have good quality parameters (high variance explained and low lack of fit). The resolved distribution maps and spectral signatures are displayed in the appendix. Below the description of the components resolved is described.

Population	Multiset images	Number of components	Variance explained (%)	LOF (%)
Control	6	5	99.8	4.6
50 µM	6	7	99.6	6.2
1000 µM	6	5	99.6	6.2

Table 2. Information and model fit parameters from the results of MCR- ALS analyzes of fluorescence images.

Tree common components (A, C and E) were resolved in the control population, in the Cd(II) 50 µM exposed population and in the Cd(II) 1000 µM exposed population. However, in the Cd(II) 50 µM exposed population, there are new components (F and G) which are not present in the rest of populations. These components may have been generated by the exposure to heavy metals.

In general, the common components have morphologically similar distribution maps and very similar spectra signatures in all multisets. This indicates the consistency of the reproducibility among cut, among samples of the same population and among populations. Figure 19 shows a control cryosection and its related global fluorescence map. The resolved pure spectra of the control population and the distribution map of the image displayed in Figure 19 are shown in Figure 20.

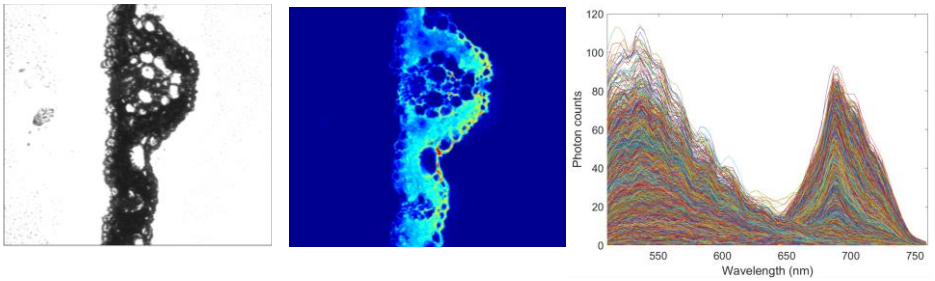

Fig. 19 On the right, the original picture of a control leaf. In the centre the fluorescence response, composed by the sum of all contributions. On the left, the fluorescence raw data.

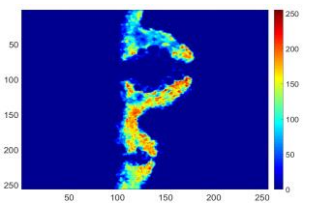

The Component A is located in the parenchyma cells. Exhibits red fluorescence (emission peak at 698 nm).

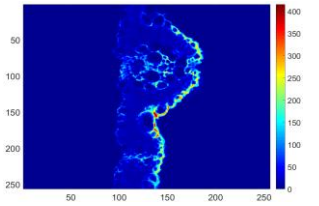

The Component B is located in the epidermis and cell walls. Exhibits blue-green fluorescence (emission peaks at 513, 523 and 535 nm).

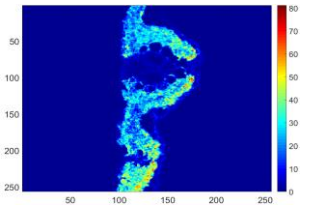

The Component C is located in the parenchyma cells. Exhibits red fluorescence (emission peak at 673 nm).

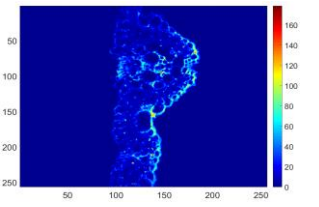

The Component D is located in the epidermis and cell walls. Exhibits green-yellow fluorescence (peaks emission at 554, 567, 585, 604 and 629 nm).

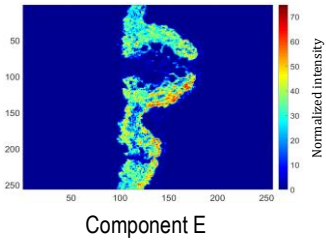

The Component E is located in the parenchyma cells. Exhibits red fluorescence (peak emission at 686 nm).

Fig. 20 Pure fluorescence signatures and distribution maps after applying the MCR – ALS method from one control cryosection.

Component B and Component D are structural components. The first one (B) is present in the epidermis and the middle lamella in vegetal cells. The middle lamella is a pectin layer which cements the cell walls of two adjoining plant cells together. The second one (D), is present in the part of the primary and secondary cell wall (Fig. 21).

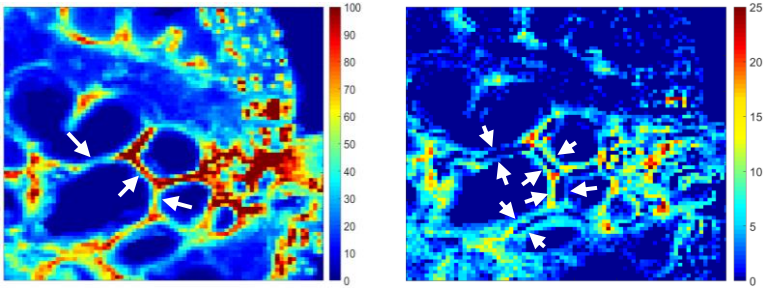

Fig. 21 On the left, the details of the distribution map of component B zoomed. This component is ubicated in the middle lamella. On the right, the details of the distribution map of component D zoomed. This component is ubicated in the primary and secondary cell wall.

These two structural components (F and G) have very similar signatures and distribution maps in control population and in Cd(II) 1000 µM exposed population. However, in Cd(II) 50 µM exposed population, there is a split in Component B and Component D in two different components. These new components are shown in Figure 22.

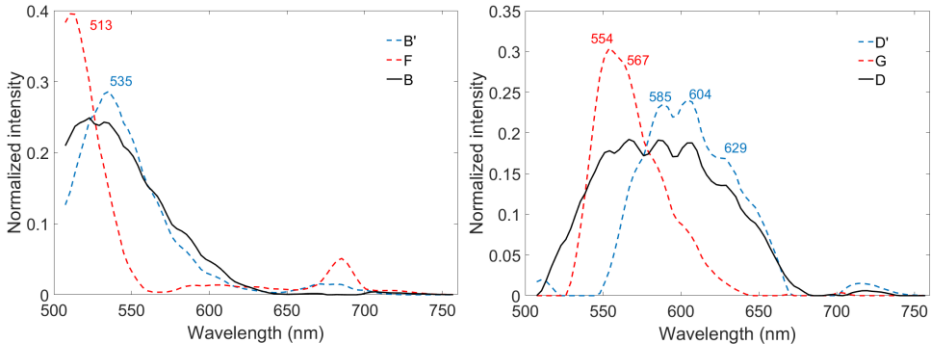

Fig. 22 On the left, Component B, with emission peaks at 513, 523 and 535 nm. The new components detected have a maximum peak at 513 nm and 535 nm respectively. On the right, Component D, with emission peaks at 554, 567, 585, 604 and 629 nm. The new components have emission peaks at 554 and 567 for one, and 585, 604 and 629 for the next one.

The new components observed G and F in Cd(II) 50 µM exposed population may originate from Components B and D as can be seen in Figure 22, but by unknown reasons these new components are separated and accumulated in very localized of the plant leaves (Fig. 23).

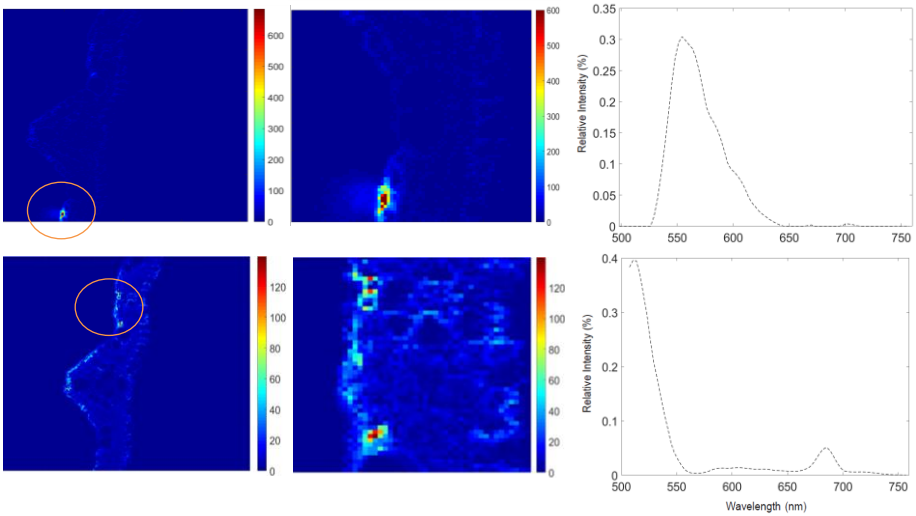

Fig. 23 On the top, the distribution map of the component G in heavy metal exposed sample. A local accumulation is founded. On the bottom, the distribution map of the component F in the same sample.

The structural components B and D, according to Lloyd Donaldson (2013)[18], may be identified as lignins. Lignin molecule is a class of complex organic polymers that form important structural materials in the support tissues of vascular plants and some algae. Lignins are particularly important in the formation of cell walls, especially in wood and bark, because they lend rigidity and do not rot easily. Lignin is formed by three different monomers: p-coumaryl alcohol, coniferyl alcohol and sinapyl alcohol. The combination of these alcohols in different proportions leads to different fluorescence spectra. In our case, it seems to be that two types of lignin were found (Fig. 24).

The differentiation between these two types is possible due to the different distribution in cryosection and the different spectra. Other chemical analyzes would be useful to confirm the presence of these components in Oryza Sativa tissues.

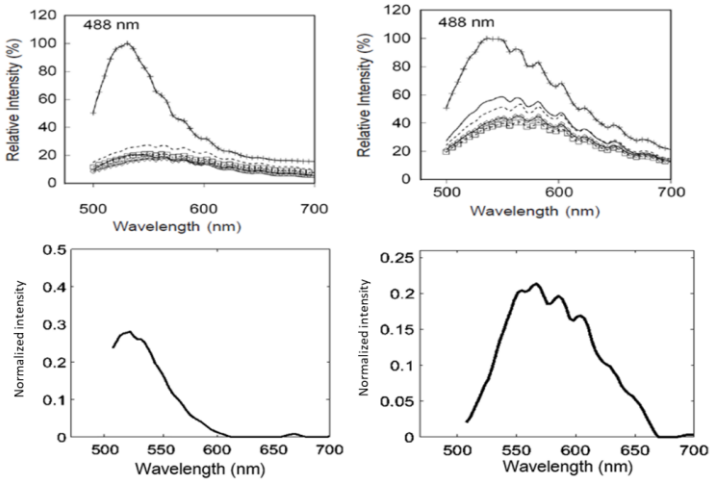

Fig. 24 On the top, two types of lignin adapted from [Donaldson, L. 2013]. On the bottom, resolved spectra of lignins by MCR – ALS.

Then, component B and component D probably are structural polymers. This reinforces the idea that the component F, G, B' and D' can be molecules that before formed part of the component B and D, and have been dissociated of the principal polymer after the exposure to heavy metals.

On the other hand, three components more were resolved (A, C and E). These components are located in the parenchyma cells. The distribution map of these components coincides with the location of chlorophylls. Then, they can be fluorophores presents in chloroplasts, such as carotenoids or chlorophylls. The component A is the most fluorescent component in the sample. The rest (C and E) have a weak fluorescence. These components are common in all images, except in some images of heavy metal exposed population (due to the less chlorophyll concentration), with emission peaks around 698 nm for A, 673 nm for C and 686 nm for E.

However, a structural difference was observed in the resolved distribution maps between component A and component C. Component A has a central distribution inside the cell, while component C has a peripheric distribution (Fig. 25).

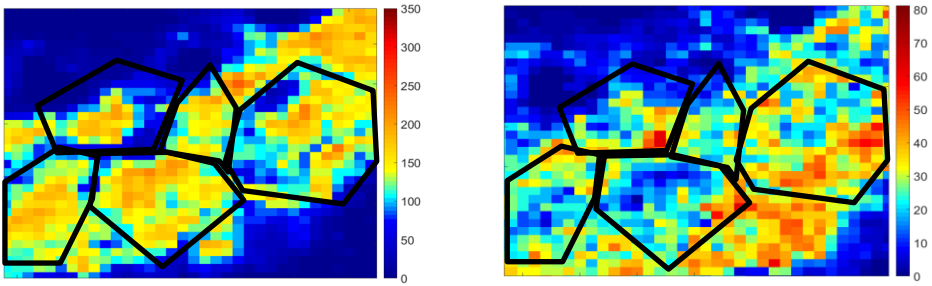

Fig. 25 Images zoomed of the same sample and same area. On the right, the distribution map of component A. On the left, the distribution map of component C.

According to the literature, chlorophyll A (Chl A) are the most fluorescent compound in red fluorescence and has a maximum emission peak around 686 nm[27]. Another fluorophore in the red fluorescence range is the chlorophyll B (Chl B). This compound is a form of chlorophyll and helps in photosynthesis by absorbing light energy. The Chl B emits around 680 nm in corn leaf[28]. Other studies found in the literature indicates that the Chl B extracted by solvents emits around 650 nm[13,29]. This contradiction may be due to the emission spectrum of the Chl B may change when it is measured in a different environment, shifting the maximum emission peak in vivo. Chl A distribution has been reported as a central distribution inside the cell, while the Chl B has a peripheric distribution[14].

This coincides with the structure shown previously in Figure 24, reinforcing the idea that component A is Chl A, and component C is Chl B.

Component E has a maximum peak at 686 nm, the same as Chl A. Then, we are faced by a contradiction: component A is the most fluorescent component, but does not have the Chl A peak (686 nm). However, the Chl emission peaks may shift in different species of plants and the component E presents a very weak fluorescence. Therefore, component A probably is Chl A.

Finally, the component E was resolved as a unknow type of chlorophyll. The distribution map presents a peripheric concentration of this component around the vessels (Fig. 26).

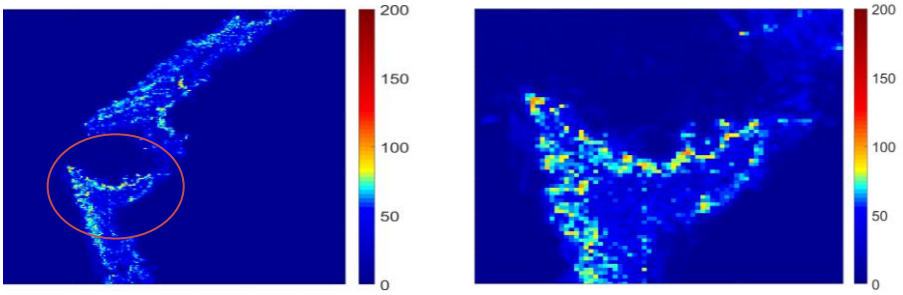

Fig. 26 An example of distribution map of the component E. It is observed the peripheric location around the vessels and epidermis.

All components and their possible identification are shown below.

Component	Identification	Experimental emission peak (nm)
A	Chlorophyll A	698
B	Type of lignin I	513, 523 and 535
C	Chlorophyll B	673
D	Type of lignin II	554, 567, 585, 604 and 629
E	Unknown chlorophyll	686
F	Segment of lignin I	513
G	Segment of lignin II	554 and 567

About the effects of the cadmium exposure on chlorophyll, significant differences were found in raw spectra. As was expected, in exposed populations the fluorescence intensity was generally low in the chlorophyll emission range (650 – 760 nm). In contraposition, the fluorescence intensity was high and reproducible among cuts, leaves and plants in all control samples (Fig. 27).

This confirms the results observed in section 7.1, where the cadmium exposed leaves were less green than control leaves due to a less chlorophyll concentration.

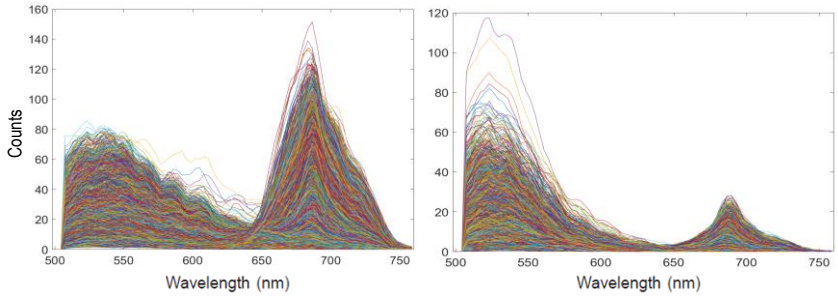

Fig. 27 On the right, raw spectra of a control image. On the left, raw spectra of cadmium exposed image.

About the changes induced by cadmium in structural components, section 7.2 describes a weakness of the samples. During the cuts in the cryostate, the vessels, in several cases, were destroyed. The accumulation and rupture of the lignin polymers observed in this work could explain the weakness observed.

In general, the visual effects observed in sections 7.1 and 7.2 agree with the chemical results obtained by combining fluorescence imaging and the MCR – ALS method.

8. CONCLUSIONS

1. About the study performed in this work: a protocol oriented to study the changes induced by cadmium exposure in Oryza Sativa Japonica Nipponbare tissues has been proposed. To do so, several steps have been carried out: a) optimization of instrumental parameters related to the fluorescence image acquisition. b) the use and the adaptation of preprocessing algorithms to improve the instrumental response. c) the use of the MCR – ALS method in order to obtain biological information and a correct interpretation of the components present in the vegetal tissue studied.
2. About the cryosection protocol: Protocol OCT – based was carried out in order to achieve 20 μm thick plant sections and preserve the morphology of biological tissues. The results indicate that OCT – protocol was adequate to achieve a good preservation of the morphology. The fact of freezing the sample allows preserving samples over long periods of time. On the other hand, OCT polymer has signal instrumental in other techniques such as Raman or NIR and requires to work with dry samples to allow the combination of the fluorescence technique with other analytical techniques.
3. About the fluorescence imaging: Fluorescence imaging allowed a fast image acquisition and a detailed map of the morphology of the leaf due to the high spatial resolution. Thus, we can observe small biological structures and understand more the biological process involved in Cd(II) exposure. On the other hand, the spectra are not especially selective as can be Raman spectra and this can hinder the complete identification of some components. The instrumental parameters used allowed obtaining good resolved spectra to be assigned and interpreted.
4. About the MCR – ALS method: MCR – ALS was a good chemometric tool to obtain information about the biological fluorophores from fluorescence images. This chemometric tool allowed differentiating components characterizing the from a spectral and spatial point view. The interpretation and identification of the results obtained from MCR – ALS method has been based on the comparison between the resolved spectra obtained and the spectra found in the literature and the morphology of the distribution maps. Three multisets (one per population) were carried out, helping the resolution of the spectra and distribution maps. The chlorophyll A and the chlorophyll B may be related with A, C and E components. The

localization of these components was established in the parenchyma cells. On the other hand, two structural components (B and D) were identified and their location was established in the vessels and the epidermis. Different kinds of lignin are candidates to be those components.

5. About the exposition to cadmium: The effect of exposure to stressors such as cadmium was evaluated in Oryza Sativa. During the growth, significant differences such as a less chlorophyll concentration in leaves were found among populations. In exposed cryosections, the biological morphology seemed to be weaker than in control cryosections. On the other hand, in raw spectra, a decrease of the intensity of chlorophyll band was founded in exposed populations. In addition, the lignin spectra seemed to be divided in exposed populations, showing accumulations in several zones of the plant tissue, maybe related with the components F, G, B' and D'.
6. About the future works: A new protocol must be developed to avoid the embed medium signal problem to achieve a multi-measurement of the same sample. This could allow us to combine several analytical techniques and collect more complete biological information about the same sample. Furthermore, exciting at lower wavelength to enlarge the emission range collected by the detector could give selective information about other components not detected. Several components of interest, such as hydroxycinnamic acids (presents as structural components in vessels o in the epidermis) have the maximum fluorescence emission peak at blue zone of the electromagnetic spectrum.

9. REFERENCES AND NOTES

(1) Bundy, J. G.; Davey, M. P.; Viant, M. R. Environmental Metabolomics: A Critical Review and Future Perspectives. *Metabolomics* **2009**, *5* (1), 3–21.

(2) Food and Agriculture Organization of the United Nations. International Year of Rice 2004: Gender and Rice. *FAO Factsheet* **2004**, Table 1, 1–2.

(3) Chang, T.-T.; Bardenas, E. A. The Morphology and Varietal Characteristics of the Rice Plant. *Tech. Bull. 4* **1965**, 40.

(4) Myburg, A. A.; Lev-Yadun, S.; Sederoff, R. R. Xylem Structure and Function. *eLS* **2013**, 1–9.

(5) Leegood, R. C. Roles of the Bundle Sheath Cells in Leaves of C3 Plants. *J. Exp. Bot.* **2008**, *59* (7), 1663–1673.

(6) Jordan, B. R. *The Effects of Ultraviolet-B Radiation on Plants: A Molecular Perspective*; **1996**. *22*, 97–162.

(7) Booij-James, I. S.; Dube, S. K.; Jansen, M. A.; Edelman, M.; Mattoo, A. K. Ultraviolet-B Radiation Impacts Light-Mediated Turnover of the Photosystem II Reaction Center Heterodimer in Arabidopsis Mutants Altered in Phenolic Metabolism. *Plant Physiol.* **2000**, *124* (3), 1275–1284.

(8) Young, A. J. The Photoprotective Role of Carotenoids in Higher Plants. *Physiol. Plant.* **1991**, *83* (4), 702–708.

(9) Pagliano, C.; Raviolo, M.; Dalla Vecchia, F.; Gabbrielli, R.; Gonnelli, C.; Rascio, N.; Barbato, R.; La Rocca, N. Evidence for PSII Donor-Side Damage and Photoinhibition Induced by Cadmium Treatment on Rice (Oryza Sativa L.). *J. Photochem. Photobiol. B Biol.* **2006**, *84* (1), 70–78.

(10) Jamila, A.M.; Jusoh, K.; Ismail, B.S.; Talip, N. Effects of Heavy Metal Exposure on the Morphological and Microscopical Characteristics of the Paddy Plant. J. Environ. Biol. **2016**, *37*, 955–963.

(11) Lagorio, M. G.; Cordon, G. B.; Iriel, A. Reviewing the Relevance of Fluorescence in Biological Systems. *Photochem. Photobiol. Sci.* **2015**, *14* (9), 1538–1559.

(12) Krause, G. H.; Weis, E. Chlorophyll Fluorescence as a Tool in Plant Physiology - II. Interpretation of Fluorescence Signals. *Photosynth. Res.* **1984**, *5* (2), 139–157.

(13) Pfarrherr, A.; Teuchner, K.; Leupold, D.; Hoffmann, P. Chlorophyll B in Solution: Fluorescence Lifetimes, Absorption and Emission Spectra as Criteria of Purity. *J. Photochem. Photobiol. B Biol.* **1991**, *9* (1), 35–41.

(14) Pedroso, M.; Sinclair, M.; Jones, H.; Haaland, D. Hyperspectral Confocal Fluorescence Microscope: A New Look into the Cell. *Microsc. Microanal.* **2009**, *15* (S2), 880.

(15) Jamme, F.; Kascakova, S.; Villette, S.; Allouche, F.; Pallu, S.; Rouam, V.; Réfrégiers, M. Deep UV Autofluorescence Microscopy for Cell Biology and Tissue Histology. *Biol.*

Cell **2013**, *105* (7), 277–288.

(16) Lichtenthaler, H. K.; Schweiger, J. Cell Wall Bound Ferulic Acid, the Major Substance of the Blue-Green Fluorescence Emission of Plants. *J. Plant Physiol.* **1998**, *152* (2–3), 272–282.

(17) Kilcrease, J.; Collins, A. M.; Richins, R. D.; Timlin, J. A.; O'Connell, M. A. Multiple Microscopic Approaches Demonstrate Linkage between Chromoplast Architecture and Carotenoid Composition in Diverse Capsicum Annuum Fruit. *Plant J.* **2013**, *76* (6), 1074–1083.

(18) Donaldson, L. Softwood and Hardwood Lignin Fluorescence Spectra of Wood Cell Walls in Different Mounting Media. *IAWA J.* **2013**, *34* (1), 3–19.

(19) Navarro-Reig, M.; Jaumot, J.; García-Reiriz, A.; Tauler, R. Evaluation of Changes Induced in Rice Metabolome by Cd and Cu Exposure Using LC-MS with XCMS and MCR-ALS Data Analysis Strategies. *Anal. Bioanal. Chem.* **2015**, *407* (29), 8835–8847.

(20) Loza-alvarez, P.; Pi, B. Trends in Analytical Chemistry Relevant Aspects of Unmixing / Resolution Analysis for the Interpretation of Biological Vibrational Hyperspectral Images. *Trends Anal. Chem.* **2017**, *94*, 130–140.

(21) Savitzky, A.; Golay, M. J. E. Smoothing and Differentiation of Data by Simplified Least Squares Procedures. *Anal. Chem.* **1964**, *36* (8), 1627–1639.

(22) Jaumot, J.; de Juan, A.; Tauler, R. MCR-ALS GUI 2.0: New Features and Applications. *Chemom. Intell. Lab. Syst.* **2015**, *140*, 1–12.

(23) Jolliffe, I. T. Principal Component Analysis, Second Edition. *Encycl. Stat. Behav. Sci.* **2002**, *30* (3), 487.

(24) Windig, W.; Guilment, J. Interactive Self-Modeling Mixture Analysis. *Anal. Chem.* **1991**, *63* (14), 1425–1432.

(25) de Juan, A.; Jaumot, J.; Tauler, R. Multivariate Curve Resolution (MCR). Solving the Mixture Analysis Problem. *Anal. Methods* **2014**, *6* (14), 4964–4976.

(26) Taylor, P.; Zhou, Q.; Wang, X.; Liang, R.; Wu, Y. Effects of Cadmium and Mixed Heavy Metals on Rice Growth in Liaoning, China. *Soil Sediment. Contam.* **2003**, *12* (6), 851–864.

(27) Ndao, A. S.; Konté, A.; Biaye, M.; Faye, M. E.; Faye, N. A. B.; Wagué, A. Analysis of Chlorophyll Fluorescence Spectra in Some Tropical Plants. *J. Fluoresc.* **2005**, *15* (2), 123–129.

(28) Jones, H. D. T.; Haaland, D. M.; Sinclair, M. B.; Melgaard, D. K.; Van Benthem, M. H.; Pedroso, M. C. Weighting Hyperspectral Image Data for Improved Multivariate Curve Resolution Results. *J. Chemom.* **2008**, *22* (9), 482–490.

(29) Thorne, S. W.; Newcomb, E. H.; Osmond, C. B. Identification of Chlorophyll B in Extracts of Prokaryotic Algae by Fluorescence Spectroscopy. *Proc. Natl. Acad. Sci.* **1977**, *74* (2), 575–578.

APPENDIX

APPENDIX

Control population

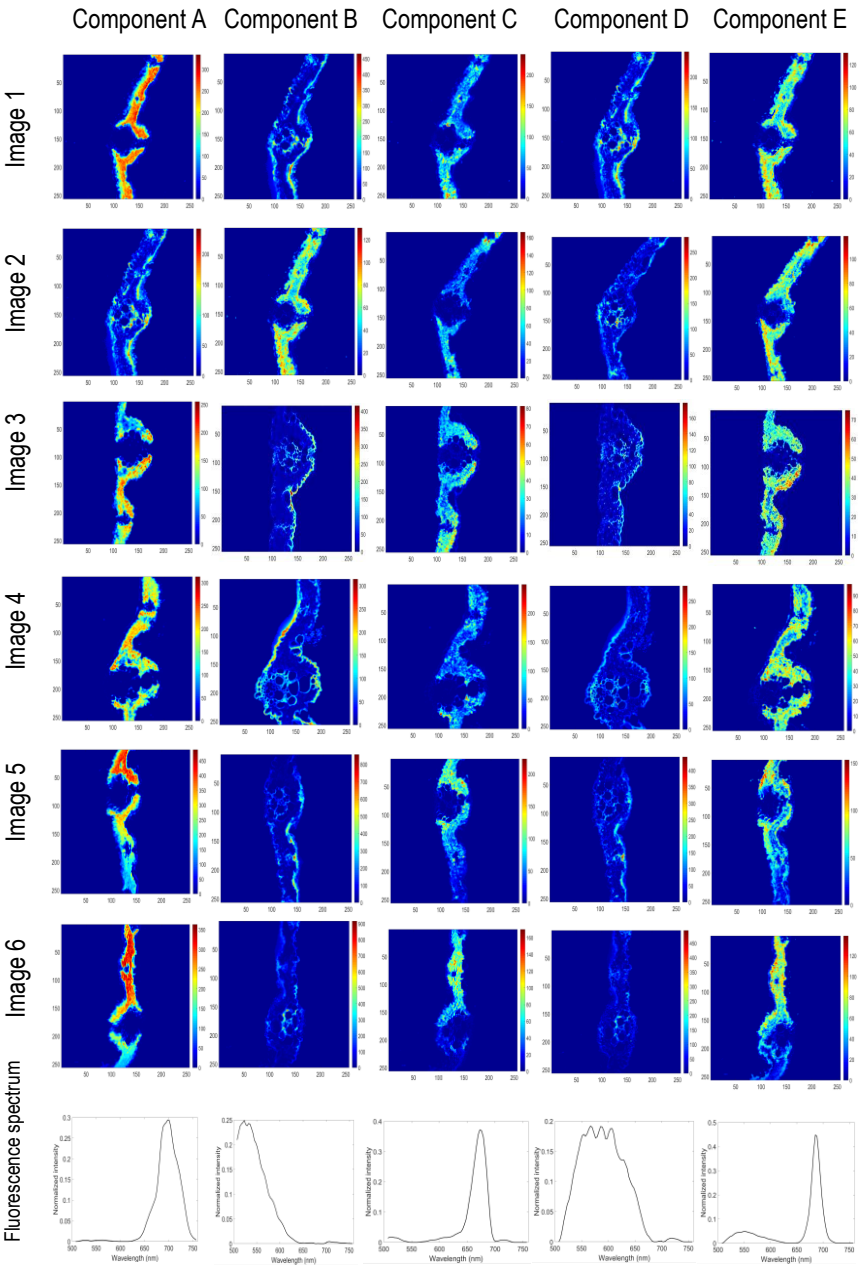

Figure S 1. MCR – ALS resolved distribution maps and spectral signatures of control population.

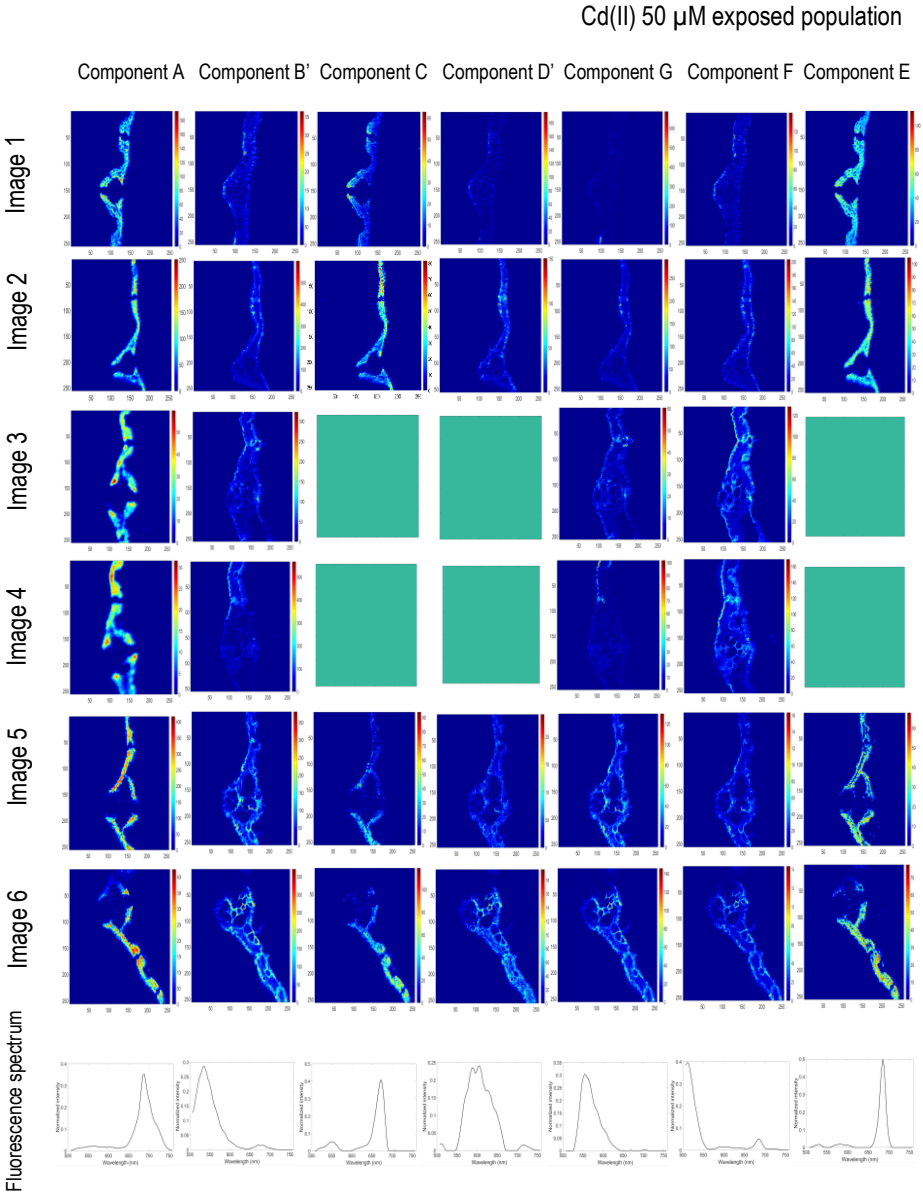

Figure S 2. MCR – ALS resolved distribution maps and spectral signatures of Cd(II) 50 µM exposed population. Green maps refer to missing compounds.

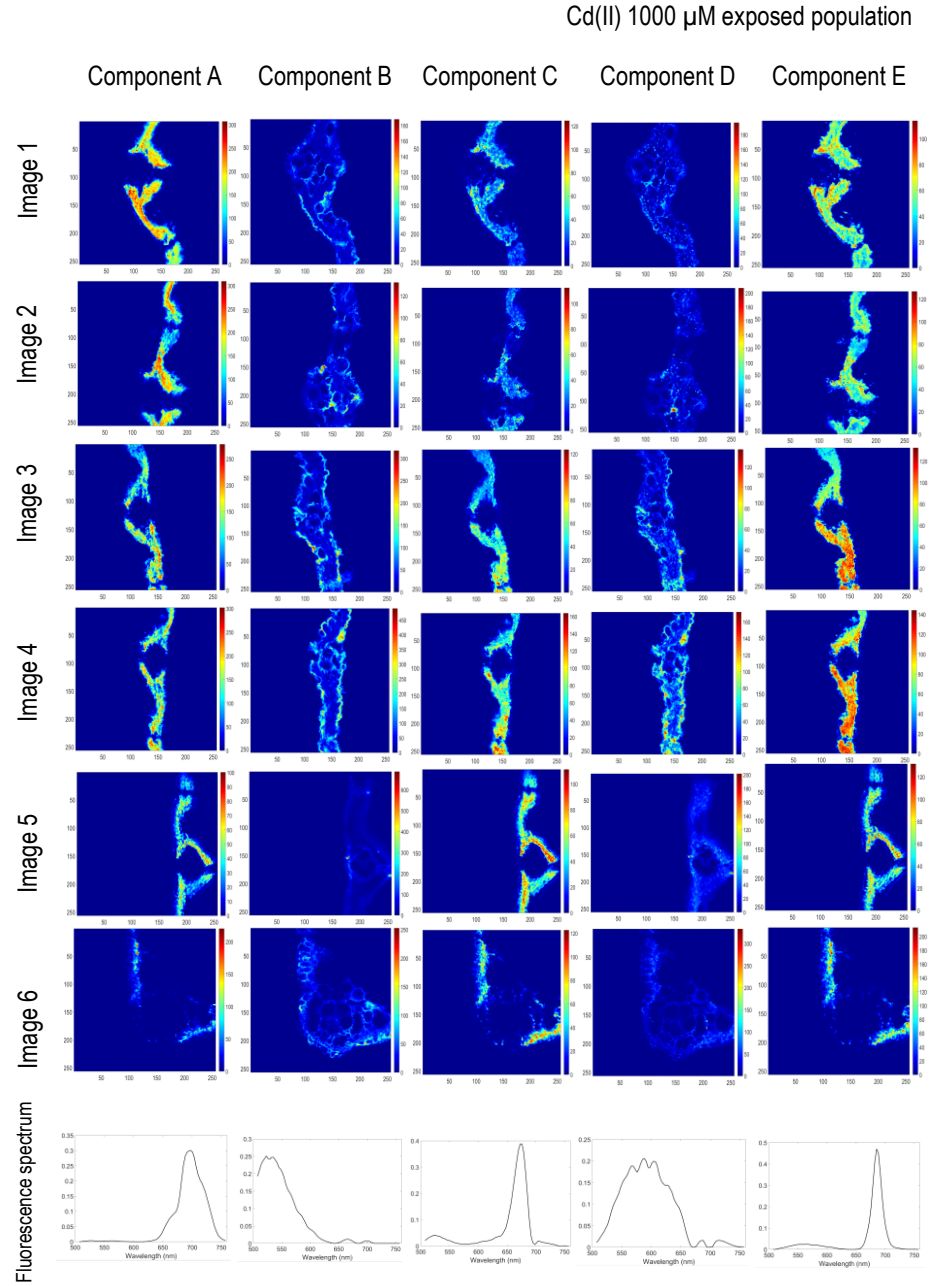

Figure S 3. MCR – ALS resolved distribution maps and spectral signatures of Cd(II) 1000 µM exposed population.